Modular modeling of Electrochemical Reactors: Comparison of CO_2-Electolyzers

Luisa C. Brée[1], Matthias Wessling[2,3], Alexander Mitsos[4,1,5]*

[1] *Process Systems Engineering (AVT.SVT), RWTH Aachen University, 52074 Aachen, Germany*

[2] *Chemical Process Engineering (AVT.CVT), RWTH Aachen University, 52074 Aachen, Germany*

[3] *DWI-Leibniz Institute for Interactive Materials, Aachen, Germany*

[4] *JARA-ENERGY, 52056 Aachen, Germany*

[5] *Energy Systems Engineering (IEK-10), Forschungszentrum Jülich, 52425 Jülich, Germany*

Keywords:

CO_2-Reduction

Reactor Design

Gas diffusion electrodes

PEM electrolysis

alkaline electrolysis

overpotential distribution

Abstract: For economic electrochemical production at industrial scale, high current densities are desired. Conversely, economic electricity utilization requires minimal overpotentials. Ultimately, product yield and composition most likely depend on both overpotential and current density. Modeling and simulation enable the detailed examination. Therefore, we develop modular mechanistic dynamic models for parts of the electrochemical membrane reactors that can be assembled to represent cell setups in order to assess their performance and optimization potential. The models include relevant overpotentials such as ohmic losses and mass transport limitations. The modelling methodology is applied to experimental CO_2 reduction data in different cell setups. The novelty of the work lies in the parameter estimation to experimental data given for very

Corresponding author: *A. Mitsos
AVT Process Systems Engineering, RWTH Aachen University, 52074 Aachen, Germany
E-mail: amitsos@alum.mit.edu

different electrode/membrane configuration as well as very different gas and liquid flow configurations. The validated models allow the analysis and detailed comparison of dominant loss terms of the reactor setups indicating optimization possibilities and potentials.

1 Introduction

Electrochemical membrane reactors can be used to produce synthetic chemicals and fuels from renewable electricity. Production at industrial scale requires economically efficient processes which in turn implies thermodynamic efficiency or equivalently minimal overpotentials. These overpotentials are influenced by the reactor setup, materials, geometries, electrodes, etc.[28] and increase towards high cell potentials due to mass transport limitations or electrode coverage by evolving product gases[47]. However, a high current density is required in order to minimize the membrane and electrode area and thus keep investment costs low[5]. An optimal operating point therefore balances high product formation at high possible current densities and high dissipation losses.

Different concepts of electrolyzer setups are under development with specific dominating overpotentials, such that depending on the type of application, one or the other setup must be selected[39]. In other words, the most beneficial combination of setup and cell potential should be found for an envisaged application.

The identification of the optimum operating point in electrochemical membrane systems is even more complex due to the fact that the product spectrum is strongly affected by the applied electrode potential. This is particularly the case in CO_2 reduction[23;39]. An electrochemical cell for the conversion of CO_2 with water splitting at the anode can produce valuable fuels and raw chemicals from CO_2[14]. Many studies revealed that this process is a promising technique to capture CO_2 released by many industrial or other processes and to prevent it from contributing to the greenhouse effect by closing the carbon cycle[14;4].

There are many remaining challenges such as catalyst selection and design[33;4], as well as device design[39]. Recently, a thorough investigation describes how different CO_2 reduction catalysts should be analyzed through standard protocols[10]. But most importantly, Verma et al.[40] show the relevance of early-stage assessments at the system level for electrochemical systems using the example

of CO_2 reduction. As in CO_2 co-electrolysis the type of product highly depends on the type of catalyst[22], many studies focus on the cathodic reactions. For instance, Silver (Ag) electrodes are well known as catalysts for CO formation (with side product H_2). Copper (Cu) electrodes are among the most studied materials for catalyzing the reduction of CO_2, in particular for the production of hydrocarbons as it is the only pure metal that is active for CO_2 reduction towards hydrocarbons and alcohols[20]. Among the heterogeneous and molecular electrocatalysts analyzed by Kortlever et al.[22], it exhibited the highest yields for hydrocarbon products with acceptable efficiencies. However, high overpotentials are needed, a variety of products are formed and hydrogen evolution competes with CO_2 reduction which reduces the Current Efficiencies (CEs, also called Faradaic Efficiencies) toward carbon-containing products[14;33]. The product spectrum is strongly affected by the applied electrode potential[23].

Besides this important fundamental comprehension of the cathodic reactions, the assessment at system level lead Verma et al. to an exchange of the typically used anode-reaction of oxygen evolution with an oxidation of glycerol − a waste stream from biodiesel production − which resulted in reduced electricity consumption by up to 53%[40]. With this publication at hand, Bardow and Wessling emphasize the importance of considering a cell modularly in order to find bottlenecks and suitable alternatives to these bottlenecks[2]. Herein, a method is therefore developed that enables the modular coupling of redox systems in order to facilitate the investigation of reactions and counterreactions individually as well as coupled.

Many studies are conducted experimentally to focus on the performance of electrochemical reactors e.g., done in Li et al.[24], Zhou et al.[48] and many more. The experimental approach requires a variety of experiments. To simplify the search for the most beneficial combination of setup and cell potential for the aimed product spectrum, research activities in the field of electrochemical cell modeling is extensive and numerous models exist for various applications, setups or even individual components. These models vary in their level of detail,

spatial resolution (0D, 1D, 2D, 3D), assumptions taken into account, etc. For instance Wu and Zhou[46] present a review on transport and performance modeling of PEM fuel cells. Although many models exist, these are often developed for a specific application. Since many options for process design and operation are possible, a modular model can help assess the performance and optimization potentials of a little known process. A comprehensive approach comparing different reactor configurations has recently been published[44], yet the model is not compared to actual data. We develop modular methodology and apply the dynamic models to own experimental data published in Vennekoetter et al.[39].

Furthermore, very little attention is yet given to the comparison of electrochemical membrane cell models showing different flow configurations. Hence, we focus here for the first time on the particular question how flow patterns can affect reactor performance and consider an electrochemical CO_2 co-electrolysis.

The modularity allows a flexible model assembly especially for such applications where the right choice in cell design is still under research. The dynamic version of this model enables to deconvolute the various phenomena occurring (e.g. parts of the phenomena presented in Roghmans et al.[34] or Rommerskirchen et al.[35]) and allows the analysis of control-strategies or demand side management, though, this is not covered in this manuscript. The models take into account the important overpotentials mostly via state-of-the art equations found in literature. The models are kept simple in order to be valid for different setups and thus to obtain a certain flexibility in terms of applying them to different reactor designs. Additionally, as we will show in the parameter estimation section, with the experimental data typically gathered by experiments, the unknown parameters for simpler models are already hardly identifiable. More detailed models invariably have more parameters and would thus further exacerbate the issue of missing data.

We use 1D models (perpendicular to the electrode) to describe the cell designs investigated here. Simulations that we performed with a 2D model, where mass transport through the buffer-layer is modeled in two dimensions (per-

pendicular and parallel to the electrode), show similar results as a 1D model. Therefore, we conclude that a 1D model is sufficient to describe the experimental data to be investigated here.

After introducing the model structure and equations, the models are validated with own experimental data and unknown parameters are determined. Especially the cathodic half-cell of the reactor is characterizing cell performance of the CO_2 reduction. Therefore, the focus is set on this cell part first in order to determine the unknown electrochemical reaction parameters of an Ag- and a Cu-electrode for CO_2 reduction. Simulations of a completely assembled reactor are then executed to characterize the behavior of each setup. Knowing the influence of relevant loss terms, individual optimization approaches can be developed for each setup.

2 Modeling

We develop modular dynamic models for electrochemical reactor components in order to assemble them to different cell setups. The models are for unpressurized reactors at room temperature and they are based on mass balances, transport equations and electrochemical kinetics thus considering the relevant overpotentials.

Note that other overpotentials than the herein described may occur, such as overpotentials in the electric connectors. For the herein analyzed setups, the considered overpotentials are assumed to be dominating.

The model is implemented in gPROMS[32] and can be downloaded here: http://permalink.avt.rwth-aachen.de/?id=280116.

2.1 Model Structure

Figure 1 shows three cell setups. Alkaline electrolysis (AEL, also called GAP-cell) is the most established technology with relatively low capital costs but high maintenance costs due to the corrosive electrolyte[17]. Polymer electrolyte membrane (PEM) electrolyzers are also commercially used, where the reactants reach the electrode through a gas diffusion layer (GDL)[17]. According to Gahleitner et al.[13], they are characterized by faster dynamics which is advantageous for coupling with dynamic and intermittent systems. However, this technology is currently more expensive than alkaline electrolysis and PEM electrolyzers have a shorter lifetime[9]. Typically, for both setups, reactants are provided in a liquid feed and gaseous products can leave the reactor. Additionally shown in Figure 1 is a combination of both setups using a PEM-halfcell at the anodic side and a GAP-halfcell at the cathodic side. This was found to be able to improve process performance for CO_2 reduction[39]. Gaseous reactants can be provided into the reactor at different inlets increasing the number of configuration-options in the GAP-halfcell setup for which examples are shown and called GAPc and GAPe. In the shown reactor combination, a gas, e.g., CO_2 can be fed through a gas

diffusion electrode (GDE). The shown GAPe-halfcell considers a dead-end flow configuration of the CO_2 inlet. More different options can be thought of and a few are discussed in Vennekoetter et al.[39]. Besides, further electrolysis technologies exist, such as solid oxide electrolysis (SOEC). However, this paper only focuses on the aforementioned types.

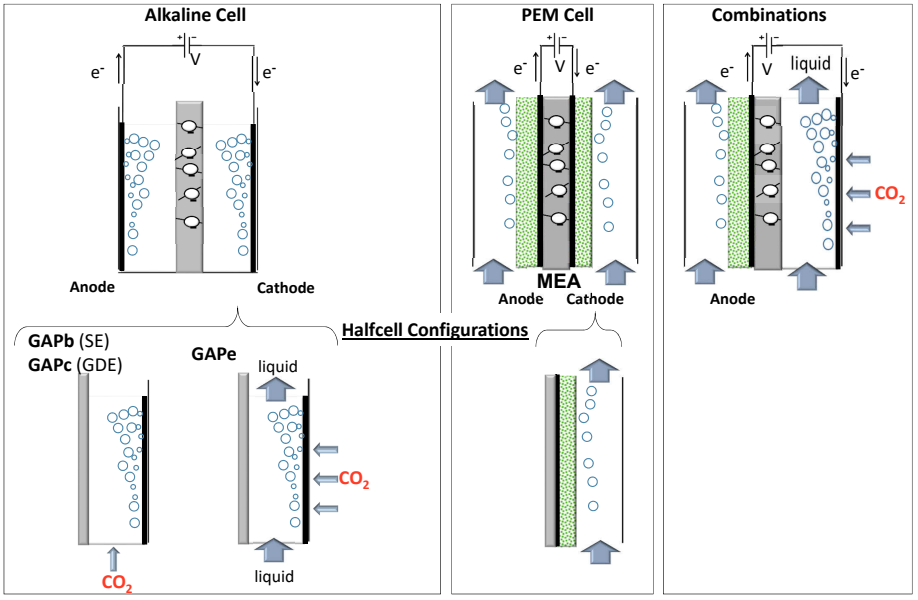

Fig. 1: Scheme of different reactor setups. Upper row shows fully assembled reactors. Lower row shows halfcell configurations with cathode and membrane for all halfcells, as well as gassing in of CO_2 for the GAP-halfcells, and a GDL with a channel for the PEM-halfcell. GAPb is equipped with a solid electrode (SE) and GAPc with a GDE.

In order to analyze, compare and optimize these cell setups, we develop modular models which can be connected according to the structure under examination. The chosen modular model parts are shown in Figure 2: One model part describes the electrochemistry including the electrochemical reactions at the electrodes. The membrane, separating both halfcells, is described by a model part. Furthermore, the provision and removal of reactants and products from/to the site of the reaction is described in the model part *mass transport* where the different cell setups are considered in one-dimensional models (perpendicular to the electrode).

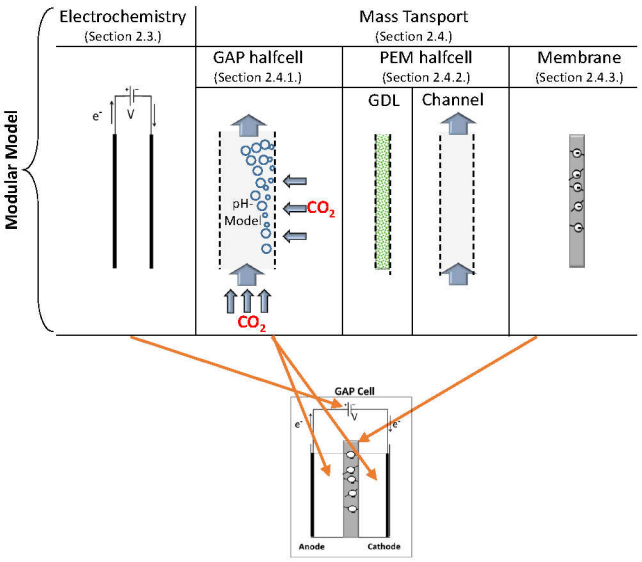

Fig. 2: Top: Moduar Models that may be used to analyze individual reactor parts or assembled to represent complete electrochemical membrane reactors. Bottom: Exemplary assembly for modeling of GAP-cell without liquid or gaseous inlets.

2.2 Assumptions

We assume ideal gases justified by the ambient operating pressure. Also, we do not account for losses due to unknown side reactions, therefore the sum over all electrochemical reactions adds up to 100 % Faradaic efficiency. In addition, the assumption of a fully hydrated membrane is made so that the manufacturer's given properties, e.g., for the conductivity, can be assumed. No cross-over of gases and a uniformly distributed current across the cell are assumed.

2.3 Electrochemistry

The core of an electrolyzer is the electrochemical unit. The total cell potential is the difference between cathodic and anodic equilibrium potentials of the electrochemical reactions plus the total overpotential η_{total} [28].

$$U_{cell} = E_{eq,C} - E_{eq,A} + \eta_{total} \tag{1}$$

$$\eta_{total} = \eta_{act,r} + \eta_{bub} + \eta_{ohm,el} + \eta_{ohm,mem} \tag{2}$$

The total overpotential is the sum of all overpotentials occurring during cell operation. Overpotentials considered in the model are activation overpotentials $\eta_{act,r}$ to force the electrochemical reactions r, overpotentials due to bubble formation η_{bub}, ohmic overpotentials of the electrolyte $\eta_{ohm,el}$ and the membrane $\eta_{ohm,mem}$ and concentration overpotentials $\eta_{conc,r}$ due to changing concentrations at the electrodes impacting each reaction. The concentration overpotential is already included in the electrode's equilibrium potentials and therefore does not occur in (2).

If more than one electrochemical reaction occurs at one electrode, one total equilibrium potential of the cell cannot be determined as the reactions differ in their equilibrium potential.

Very often, experiments aim to focus on one electrode only, which then is called working electrode. Especially for Co-Electrolysis, the cathode is under examination and experimental results often present the voltage of the cathodic halfcell with iR-drop compensation. We assert that the change in ohmic resistivity of the electrolyte at different cell potentials and overpotentials due to bubble formation is considered in the iR-compensation. The electrode (cathode) potential E_C then is only depending on the equilibrium potential $E_{eq,r}$ of each electrochemical reaction r as well as the activation potential $\eta_{act,r}$ of the reactions at the respective current density:

$$E_C = E_{eq,r} + \eta_{act,r}. \tag{3}$$

As we assume that the electrochemical reactions are taking place in parallel, the electrode potential applies to each reaction in parallel. We use the concentration-dependent equilibrium potential for each reaction at the electrode calculated by the Nernst equation[28].

$$E_{eq,r} = E_{0,r} + \frac{R \cdot T}{z_r \cdot F} \cdot \ln \frac{\Pi a_{ox,r}^{\nu_{ox,r}}}{\Pi a_{red,r}^{\nu_{red,r}}} \tag{4}$$

$E_{0,r}$ is the specific standard reduction potential, z_r the number of electrons

transferred in reaction r, $\nu_{ox,r}$ and $\nu_{red,r}$ are stoichiometric coefficients of the oxidized and reduced species in the electrochemical reactions and a_{ox} and a_{red} are the activities of the oxidized and reduced species on the surface of the electrode. The activities account for changing concentrations at the site of the concentration arising if the electrochemical reactions are faster than mass transport. This change is explicitly represented by the concentration overpotential η_{conc}, as this depends on the concentration difference between the bulk phase and the electrode surface[43]. We calculate it by

$$\eta_{conc,r} = E_{eq,r} - E_{eq0,r} \tag{5}$$

where $E_{eq0,r}$ is the equilibrium potential for reaction r with the inlet concentrations. Note that this established definition of overpotential convolutes two aspects of concentration differences: Different concentrations in the bulk and at the electrode due to mass transport limitations, and changes in the bulk from the inlet concentrations that might occur at very high current densities, for slow liquid feeding rates or in batch reactors.

The activity of species i can be related to the concentration c_i via $a_i = f_i \cdot c_i$, where f_i is the activity coefficient of species i[28]. As activity coefficients tend to unity at low concentrations, activities in the Nernst equation are replaced by simple concentrations except for the solvent water, whose activity is set to one.

The conversion of each electrochemical reaction is typically calculated by an overall rate equation, the Butler-Volmer equation[18]

$$j_r = j_{0,r} \cdot \left(\exp\left(\frac{\alpha_r \cdot z_r \cdot F \cdot \eta_{act,r}}{R \cdot T} \right) - \exp\left(\frac{(1-\alpha_r) \cdot z_r \cdot F \cdot \eta_{act,r}}{R \cdot T} \right) \right). \tag{6}$$

where $\eta_{act,r}$ is the activation overpotential. α_r is the charge transfer coefficient and $j_{0,r}$ the reference exchange current density. The latter two are individual parameters of each electrochemical reaction. For some electrode-electrochemical reaction combinations values can be found in literature, but for many, e.g., for Co-electrolysis, they are uncertain. Therefore, these parameter values will be

estimated in our study.

The total current density of the electrode is the sum of each reaction's current densities and is also equal to the total cell current density:

$$j_{cell} = \sum_r j_r.$$

The current efficiency, i.e., the fraction of the current density of each electrochemical reaction of the total current density, is calculated by

$$CE_r = \frac{j_r}{j_{cell}}.$$

Ohmic overpotential

Ohmic overpotentials are caused by the resistance to the flow of electrons or ions and occur in all components with flow of ions or electrons. According to Ohm's law, we correlate the ohmic overpotential linearly proportional to the current density j by the material specific conductivity κ and the thickness X of that material for the membrane as well as for the liquid electrolytes in the GAP-halfcells via:

$$\eta_{ohm} = X \cdot \frac{j}{\kappa}. \tag{7}$$

2.4 Mass Transport

As described above, the different cell setups are distinguished by various configurations of provision and removal of reactants and products from/to the site of the reaction. We consider two different halfcell-types (PEM- and GAP-halfcell) and the membrane. The GAP-halfcell can have different designs depending on the location of feed inlet or position of gas-injection if these exist at all. The halfcell-models can be individually analyzed or assembled with the other necessary parts to represent a whole electrolyzer. They are connected to the electrochemistry model by the molar consumption and production rate of the reactants and products by Faraday's law as the current density determines the

conversion of each species i in the electrochemical reactions r[18]

$$n_i = \frac{A}{F} \sum^{r} \frac{j_r \nu_{i,r}}{z_r}.$$

If mass transport of reactants to the site of the reactions and removal of the products is fast, concentration changes are low so that high current densities can be reached by relatively low activation overpotentials. This is influenced by the reactor setup and the employed materials. Furthermore, the activities of all reacting entities at the electrodes are calculated within this model part and influence the equilibrium potential in Eq. (4).

2.4.1 GAP-halfcell

In a GAP-halfcell, the electrode is immersed in an ionic solution. Mass transport effects that may occur are diffusion, migration and convection. The influence of migration to mass transport in an ionic solution is often considered minor, e.g., Tobias et al.[38] report that in sufficient excess of inert electrolyte the transference number of the species participating in the electrode reaction may be made negligibly small and migration need not be considered.

Here, we model mass transport through the electrolyte via mass balances taking into account a lumped mass transfer. The corresponding transport parameter will be estimated in the case study summarizing the aforementioned effects of diffusion, migration and convection. Mass transport limitations cause the concentration of reactants to decrease and of products to increase leading to concentration overpotentials. Also considered in the model is ionic equilibrium with pH-calculation.

All GAP-halfcell configurations are modeled via the same equations for the bulk phase. They are distinguished by two integer variables e_{bs} and e_{ss} indicating if CO_2 is provided via gassing in by side stream or by bottom stream - if provided at all.

We set up a 1D-model where the axis perpendicular to the electrode is ana-

lyzed. The component balances for each species i are modeled by

$$\dot{c}_i = \underbrace{n_{pH,i}}_{\text{IonicEquil.Rctn}} + \underbrace{\frac{\partial c_i}{\partial x}\left(D_i \frac{\partial c_i}{\partial x}\right)}_{\text{Lumped Mass Transport}} + \underbrace{n_{el,i}}_{\text{El.Chem.Rctn}} + \underbrace{n_{mem,i}}_{\text{Transp.Membrane}} + \underbrace{e_{bs} \cdot k_{CO2} \cdot (c_i - c_{i,0})}_{\substack{\text{CO}_2\text{-gassing} \\ \text{bottom stream}}}$$

considering changes of every species's concentration c_i due to the electrochemical reactions with $n_{el,i}$ (c.f. Section 2.3) as well as change of concentration due to the dissociation reactions in the pH-model $n_{pH,i}$ (c.f. Section pH-Model) and a transportation term representing diffusion, convection and migration of species i. The CO_2-concentration is further influenced by a possible bottom stream which is the case when CO_2 is gassed in from the bottom as in GAPc. The integer variable e_{bs} sets this stream on and off and k_{CO2} characterizes the dissolution of CO_2. Depending on the application as anode or cathode, the membrane lies on one side and the electrode on the other ($x = 0$ or $x = X$). This mass flow from/to membrane or due to the electrochemical reactions is introduced into this model part via the source terms $n_{el,i}$ and $n_{mem,i}$. $n_{el,i}$ and $n_{mem,i}$ are zero in the bulk.

pH-Model

With the initial electrolyte concentration, the pH in the liquid phase can be adjusted according to the ionic equilibrium. Additional species can influence the pH as these might dissociate in aqueous solutions into ions, like CO_2 does[36]. When the electrochemical reactions take place, the initial concentrations - especially at the reactive surface - might change, though always maintaining the ionic equilibrium. These concentration changes again have an influence on the activation overpotentials of the electrochemical reaction rates. Botz et al.[6] reported that directly at the electrode, especially in the three-phase boundary of gas diffusion electrodes, local changes in ion activities and the pH-value might have a particular influence on the reaction rates of electrochemical reactions. The consideration of the ionic equilibrium equations balancing all ionic species therefore is important for the description of an electrochemical cell. Note that the concentration changes and therefore pH-values are highly influenced by the

parameters characterising mass transfer.

The pH-system is modeled according to the modeling approach of acid-base-equilibrium presented by Walz et al.[42] with the source term $n_{pH,i}$ for each species i due to the dissociation reactions in the pH-model and the equilibrium equations with the dissociation constants $K_{r_{pH}}$ of the ionic equilibrium reactions r_{pH}:

$$n_{pH,i} = \sum^{r_{pH}} \left(\nu_{r_{pH},i} \cdot r_{r_{pH}}\right) \tag{8}$$

$$K_{r_{pH}} = \prod^{i} \left(c_i^{\nu_{r_{pH},i}}\right) \tag{9}$$

Here, $\nu_{r_{pH},i}$ is the stoichiometric coefficient of each species i in each dissociation reaction r_{pH}. $r_{r_{pH}}$ is the rate of each dissociation reaction r_{pH}. $K_{r_{pH}}$ are the dissociation constants for each corresponding dissociation reaction and can be taken from literature.

The above described 1D-PDAE system is discretized in gPROMS via the software's centered finite difference method (with order of approximation equal to 2 and 6 discretization intervals) resulting in a DAE-system. DAE-systems are characterized by the differential index[8]. The formulation presented above results in a high index-problem as the equilibrium equations for the pH-calculation are not explicit in the reaction rates. Executing an index reduction by differentiating each equilibrium equation with respect to time, reveals a hidden equation that can be solved explicitly for the corresponding equilibrium rate[42].

Boundary Conditions

Neumann boundary conditions are imposed.

$$-D_i \frac{\partial c_i}{\partial x} \cdot A_{el} = \underbrace{n_{pH,i}}_{\text{IonicEquil.Rctn}} + \underbrace{n_{el,i}}_{\text{El.Chem.Rctn}} + \underbrace{n_{mem,i}}_{\text{Transp.Membrane}} + \underbrace{e_{ss} \cdot k_{CO2} \cdot (c_i - c_{i,0})}_{\substack{\text{CO}_2\text{-gassing} \\ \text{side stream}}} \tag{10}$$

The CO_2-concentration is further influenced by a possible side stream which is the case when CO_2 is gassed in through a GDE as in GAPe. The integer

variable e_{ss} sets this stream on and off, k_{CO2} characterizes the dissolution of CO_2.

Evolving product gases are assumed to be dissolved in the liquid with a fixed liquid concentration in all simulation studies. This is true if these gases are present with a constant partial pressure in the reactor, which can be assumed if the current efficiencies are constant. Especially for CO_2 reduction this assumption is not valid. This should be further analyzed in the future as changing liquid concentrations of the products has an impact on the equilibrium potential of the electrochemical reactions and thus an impact on the production rates. For now, this influence is neglected.

2.4.2 PEM-Halfcell Model

The PEM-halfcell model consists of a model for the channel and the gas diffusion layer. The gas diffusion layer in a PEM-cell ensures transport of reactants and reaction products between inlet channel and the catalyst layer of the membrane. Furthermore, it distributes the current evenly and provides mechanical strength for the electrode membrane assembly. Mass transport is modeled by a component balance for each species i considering convection and Fick's diffusion as well as a source term at the GDL's boundaries:

$$\dot{c}_i = \underbrace{\frac{\partial c_i}{\partial x}(D_i \frac{\partial c_i}{\partial x})}_{diffusion} + \underbrace{n_{el,i}}_{\text{El.Chem.Rctn}} + \underbrace{n_{channel,i}}_{\text{Transp.Channel}} \tag{11}$$

$\dot{n}_{channel}$ describes mass transport to and from the inlet and outlet channel and depends on the concentration gradient between GDL and channel. $\dot{n}_{el}$ is calculated in the electrochemical model depending on transport through the membrane and reactions at the electrodes. Convection is assumed to be negligible here. According to Newman[28](p.533) the effective diffusion coefficients D_i in the porous structure of the GDL are given by:

$$D_i = D_{ref,i}\epsilon^{1.5} \tag{12}$$

with the reference diffusion coefficient $D_{ref,i}$ and the GDL's porosity ϵ.

The channel's task in the PEM-halfcell is to provide the reactants and to allow the streaming out of the product gases to the gas diffusion layers. The stream entering the channel is known concerning volume flow and concentration, while the outgoing stream and the concentrations along the length of the channel are calculated via a component balance for each species i assuming a constant volume:

$$\dot{c}_i = \underbrace{-\frac{\partial}{\partial x}(c_i \vec{v})}_{convection} + \underbrace{\frac{\partial}{\partial x}(D_i \frac{\partial c_i}{\partial x})}_{diffusion} + \underbrace{\dot{n}_{channel,i}}_{source\ term} \tag{13}$$

The flow from channel to GDL for each species is driven by the concentration gradient and uses the convective parameter h_{conv}:

$$\dot{n}_{channel,i} = h_{conv}(c_{i,GDL} - c_i) \tag{14}$$

2.4.3 Membrane

The membrane separates both halfcells of the reactor allowing for ion transport. Usually transport of ions through the membrane is fast and herein assumed instantaneous. If water is present, a water flux through the membrane occurs that can not be neglected. This water flux is reported to be governed for Fuel Cells by[15]: (i) electro-osmotic drag of water by protons, (ii) diffusion driven by a concentration gradient and (iii) convection if a pressure gradient is present. These effects occur in electrolysis as well as partly in opposite directions.

Herein, a mass flow of water through the membrane is calculated via:

$$\dot{n}_{H2O} = \dot{n}_{H2O,drag} + \dot{n}_{H2O,diff}$$

considering a flow due to electro-osmotic drag and a flow due to diffusion (In this study, no pressure gradient is considered.). Electro-osmotic drag in membranes describes the transport of water (or other solvents) due to the movement of ions

through that membrane due to an electric field[45]. Electro-osmotic drag has been investigated extensively both experimentally and in simulations[15]. Simplified models concentrate on defining the drag coefficient ξ that quantifies the number of water molecules transported through the membrane by each proton, that migrates through the membrane. The molar flow of water by electro-osmotic drag can then be defined proportional to the current by[15]:

$$\dot{n}_{H2O,drag}(y) = \xi \cdot \frac{A}{F} \cdot j_{total}\,(y)\,.$$

Diffusion is driven by concentration gradients between anodic and cathodic side of the membrane and can be modeled by:

$$n_{H2O,diff} = \frac{D_{mem,H2O}}{X}\,(c_{H2O,C} - c_{H2O,A})$$

Here $D_{mem,H2O}$ is the diffusion coefficient of the membrane for water, X the thickness of the membrane and $c_{H2O,A/C}$ the concentrations of water at the anodic and cathodic boundary of the membrane.

Even if proton transport is assumed to be instantaneous, an ohmic loss in the membrane is calculated according to Eq. (7).

2.5 Influence of Electrode Coverage by Product Gases

The physical blocking of the electrodes in both setups by the gaseous reaction products is identified as one of the major sources for undesired overpotentials at high current densities according to Yang et al.[47]. We described a first approach in order to model this effect in Brée et al.[7]. As we will see later, in the herein considered case study, the overpotential due to electrode coverage by product gases is only minor as it only occurs at higher current densities. Thus, experimental data for higher current densities/cell potentials is needed to correctly parameterize the influence of electrode coverage.

3 Comparison of Reactors for CO_2 Reduction

We use experimental data gathered by Vennekoetter et al.[39]. They develop a design strategy for an electrochemical membrane reactor for different cell designs aiming for the reduction of CO_2 to hydrogen and carbon monoxide (CO) employing an Ag-electrode and additionally to ethylene (C_2H_4) employing a Cu-electrode. The considered electrochemical reactions are for the Ag-cathode:

$$2H^+ + 2e^- \rightleftharpoons H_2 \qquad E_0 = 0V \tag{RH2}$$

$$CO_2 + 2H^+ + 2e^- \rightleftharpoons CO + H_2O \qquad E_0 = -0.103V \tag{RCO}$$

and for the Cu-cathode additionally the reaction to C_2H_4 with:

$$2CO_2 + 12H^+ + 12e^- \rightleftharpoons C_2H_4 + 4H_2O \qquad E_0 = 0.079V \tag{RC2H4}$$

The reactors are lab-scale (with electrode areas of $4.5-20cm^2$) and the assembly has not been designed for optimal performance.

In the experimental data, some data-sets do not reach 100% Faradaic efficiency. Especially in the case of CO_2 reduction on Cu-electrodes, the error is high. Various references in literature agree that more electrochemical products than H_2, CO and C_2H_4 are produced. Apart the electrochemical reactions considered in Vennekoetter et al.[39] also the production of methane, formate, ethanol, n-propanol and more are reported[23;37;25;19]. Since the experimental data is far from 100% Faradaic efficiency, we introduce an additional electrochemical reaction for the Cu-electrode, that accounts for side reactions to products P that were not detected in Vennekoetter et al.[39]

$$2CO_2 + 2H^+ + 2e^- \rightleftharpoons P \qquad E_0 = 0V \tag{RP}$$

Note that a potential impact of the products P on the ionic equilibrium calculation is not considered in our models. Especially when the proportion of P is

high, it will affect the results and therefore, with such an assumption, the model is only valid for data close to 100% faradaic efficiency which is the case for the herein considered Ag-electrode. However, in the case of the Cu-electrodes, the product spectrum is broad and P is representative for a whole range of products. Within the data at hand, these additional products were not further specified making this approach the only possible solution.

In the beginning of this chapter we introduce the chosen setups and initial conditions. Then, we only consider the electrochemistry-model first in order to determine the reaction parameters for the Ag-electrode and the Cu-electrode. Extending the simplified model by mass transfer allows for determination of the mass transport kinetics. Assembly of the halfcells to a complete electrochemical reactor allows for analysis of the overpotential distribution uncovering improvement approaches.

3.1 Cell Setups and Initial Conditions

3.1.1 PEM-Halfcell

In the herein presented manuscript, the PEM-halfcell is only used as anodic halfcell. The geometric and material parameters are summarized in the SI (Table 1). The initial values are chosen to be $c_{0,H2O} = 55$ mol/l and of Protons and Oxygen to unity.

3.1.2 GAP-Halfcell

The different GAP-halfcell configurations shown in Figure 1 are analyzed with the geometric and material parameters summarized in the SI (Table 1). The initial values are deduced from the initial conditions of the real experiment conducted by Vennekoetter et al.[39]. They used a 0.5M potassium sulfate (K_2SO_4) electrolyte with gassing in of CO_2. To determine the initial concentrations in the cathodic halfcell, the ionic equilibrium is calculated for the mixture of water, 500 mol/m^3 K_2SO_4 and the respective concentration of dissolved CO_2 via the

following dissociation reactions:

$$\text{Dissociation of water:} \quad \mathrm{H_2O} \leftrightarrow \mathrm{OH^-} + \mathrm{H^+} \tag{15}$$

$$\text{addition of } \mathrm{CO_2}: \quad \mathrm{HCO_3^-} + \mathrm{H^+} \leftrightarrow \mathrm{CO_2}(aq) + \mathrm{H_2O} \tag{16}$$

$$\mathrm{HCO_3^-} + \mathrm{H^+} \leftrightarrow \mathrm{H_2CO_3} \tag{17}$$

$$\mathrm{CO_3^{2-}} + \mathrm{H^+} \leftrightarrow \mathrm{HCO_3^-} \tag{18}$$

$$\text{addition of } \mathrm{K_2SO_4}: \quad \mathrm{K_2SO_4} \rightarrow 2\mathrm{K^+} + \mathrm{SO_4^{2-}} \tag{19}$$

$$\mathrm{SO_4^{2-}} + \mathrm{H^+} \leftrightarrow \mathrm{HSO_4^-} \tag{20}$$

$$\mathrm{HSO_4^-} + \mathrm{H^+} \leftrightarrow \mathrm{H_2SO_4} \tag{21}$$

We consider the dissociation of water, and according to Roughton et al.[36], the dissociation of CO_2 in aqueous solutions to carbonic acid first and then to bicarbonate, which then dissociates in water. Furthermore, we consider the dissociation of potassium bicarbonate in water. The respective dissociation constants at 25°C are given in the SI.

Ideal mass transfer according to Henry's law from the gas phase into the liquid phase would lead to a concentration of CO_2 $c_{0,\mathrm{CO2}} = 0.33\mathrm{mol/m^3}$ and a pH of 4.2. The actual pH data in the experiments is given in Vennekoetter et al.[39] for chosen setups and even for the lowest applied cell potential deviates from this ideal value. Therefore, we deduce the initial pH-value for the entire liquid phase from the experimental data measured in the bulk of setup GAPb (this is the same setup as the herein called GAPc just with a different electrode) and GAPe. To this end, we have approximated the pH-values over the current density with polynomial trendlines as shown in Figure 9 and extrapolated the pH-values down to j=0mA/cm^2. From these pH-values we have calculated the initially dissolved concentration of $c_{0,CO2,b} = 0.0016\mathrm{mol/m^3}$ for GAPb and $c_{0,CO2,e} = 0.155\mathrm{mol/m^3}$ for GAPe. The pH-value is the same in the entire liquid phase at zero current as this indicates no net reaction at the

electrodes and thus no concentration gradients.

3.2 CO2 Reduction in GAPc-Halfcell with Cu-Electrode

We conduct a parameter estimation for the unknown electrochemical reaction parameters α and j_0 for all electrochemical reactions occurring at a Cu-electrode ((RH2), (RCO), (RC2H4), (RP)) and the mass transport coefficients in a GAPc-halfcell based on experimental results taken from Vennekoetter et al.[39].

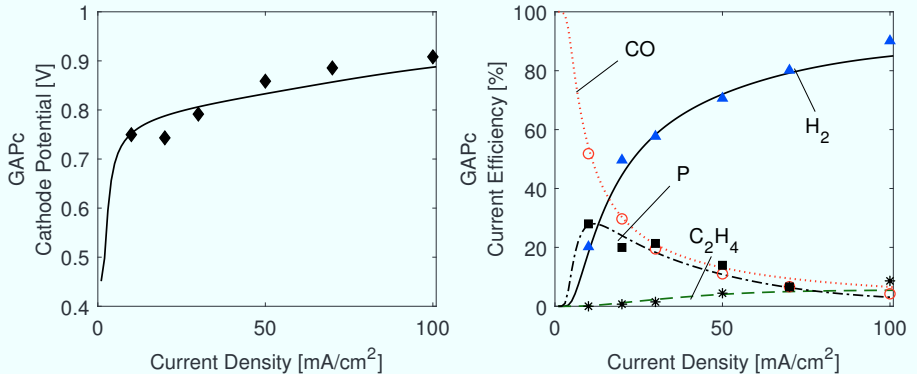

Fig. 3: Experimental[39] and simulated polarisation curve (left) and Current Efficiencies (right) for CO_2 reduction in GAPc-halfcell with a Cu-electrode. The following products were measured in the experiment and taken into account in the simulation: CO(○), H2(▲), C2H4(∗), P (■).

Table 2 in the appendix presents the estimated parameter values and the confidence intervals of the parameter values. Results of the parameter estimations with an Ag-electrode in a GAPe halfcell and for both electrodes in a GAPc-halfcell are shown in the Appendix. As shown in Figure 3, especially the current efficiency can be well represented by the model and the estimated parameters. However, the large 95% confidence intervals of the parameter values indicate that the parameters can not be identified. Identifiability of a parameter means that an unknown model parameter can be uniquely estimated based on experimental data[41]. We postulate that herein the parameters to be estimated are not identifiable. To analyze identifiability of the parameters various meth-

ods exist, which are reviewed in detail by Miao et al.[26]. In other words, the cell behavior can be described by the model, but more experiments are needed in order to exactly determine the values of the unknown parameters.

3.3 2-Stage Parameter Estimation

In the previous section, the unknown parameters of one reactor were determined all at once which leads to large confidence intervals. Reducing these intervals can be achieved by fixing chosen parameters or by expanding the number of experiments used in the estimation[41]. In the following, we combine experimental data of different reactors.

3.3.1 Determining the Electrochemical Reaction Parameters

Vennekoetter et al.[39] mainly show polarization plots for the working electrode by potentials vs. the reference electrode (SHE) and with IR-drop compensation. Therefore, only Eq. (3) is needed for calculation of the shown potentials. At low current densities it can even be assumed that the electrochemical reaction rates are still low and mass transport suffices not affecting the concentration overpotential. We therefore keep the concentrations of the species fixed for the determination of the electrochemical reaction parameters. For the estimation, experimental data for current densities below $30\mathrm{mAcm}^{-2}$ was utilized in order to exclude the mass transport limiting phenomena possibly arising at higher current densities - especially for CO_2 transport.

We calculate the activation loss, which then is the single occurring overpotential, via the Butler-Volmer equation (6) and use experimental results for nonlinear regression to estimate the reaction specific transfer coefficients α and exchange current densities j_0.

We assert that the electrochemical reaction parameters are the same in each setup employing the same electrode. As the equilibrium potentials are only reaction dependent and independent of the utilized electrode, differences in potentials can therefore only depend on concentration overpotentials. The elec-

trochemical reactions take place in parallel according to Eq. (3) which can be rewritten with Eq. (4) to:

$$E_C = \underbrace{E_{0,r}}_{fix} + \underbrace{\frac{R \cdot T}{z_r \cdot F}}_{fix} \cdot \ln \frac{\Pi \alpha_{ox}^{\upsilon_{ox}}}{\Pi \alpha_{red}^{\upsilon_{red}}} + \underbrace{\eta_{act,r}}_{f(j_{cell},\alpha,j_0)} \quad . \tag{22}$$

For estimation of the parameters a maximum likelihood formulation was evaluated by gPROMS[32] to minimize the error between simulation and experiments.

Results for the GDE employed in GAPc and GAPe

In their setup GAPc and GAPe, Vennekoetter et al.[39] use the same Nafion-bonded electrodes for CO_2 reduction. As the pH-values were not measured for GAPc, we assume that the initial concentrations are the same as in their setup b) as the reactor design is the same except for the difference in electrode-type which has no impact on initial concentrations.

We estimate the reaction kinetics of a Nafion-bonded Ag-electrode as well as of a Nafion-bonded Cu-electrode with the parameters listed in the Appendix in Table 3. The experimental data points utilized for these parameter estimations are visualized in Figure 4 where they are shown together with the simulation results of the complete 2-stage-parameter estimation. The predicted cathode potential E_C of the Ag Nafion-bonded electrode matches the experimental results for low current densities quite well. Also, the current efficiencies can be described by the herein presented approach. The same applies to both setups equipped with a Cu Nafion-bonded electrode.

According to Eq. (22), the results strongly depend on the species's activities and therefore in this section on the initial concentrations. Some of the parameters still have large confidence intervals and thus were not identified. This might be due to the formulation of the Butler-Volmer equation (6) in which the parameters α and j_0 are strongly correlated. The correlation may be reduced by reformulation of that equation or by estimating the parameters based on experiments conducted at different temperatures.

The determined values differ from the before estimated values. This may also be due to the fact that the parameters are not identified. The confidence interval of the parameter values are large. Another reason may be that the herein described model does not suffice for the description of the underlying phenomena and therefore does not adequately represent the experiment. As it was already stated in the introduction, the mechanisms of CO_2 reduction are not completely understood yet. However, with the data at hand, the model cannot be detailed.

3.3.2 Transport Kinetics for GAPc and GAPe

The determined electrochemical reaction parameters are now used in the halfcell models considering mass transport. Here, higher current densities are taken into account. Then, only the relevant transport parameters need to be estimated for each reactor setup. The simulation results are plotted in Figure 4 with the parameters determined in the estimation (Appendix, Table 4).

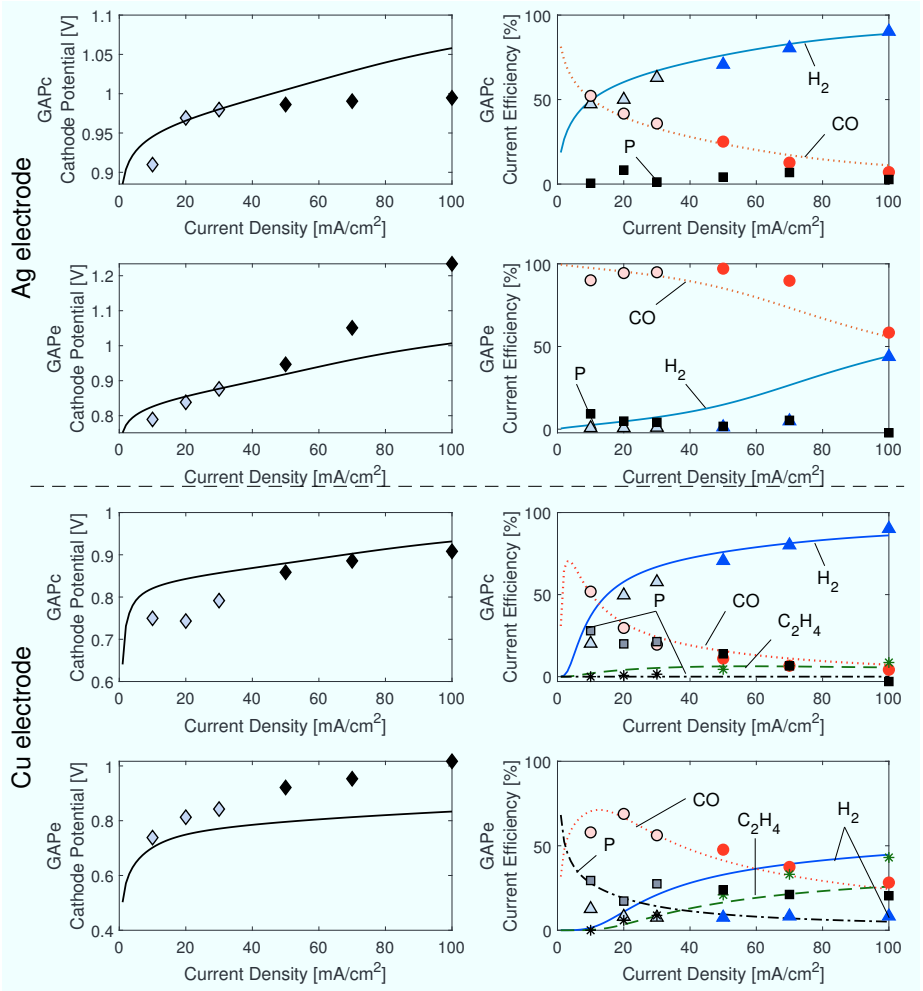

Fig. 4: Polarisation curves and Current Efficiencies for GAPc-halfcell and GAPe-halfcell with Ag- and Cu- electrode. Colored symbols is experimental data[39] (full color: used for estimation of D_{ref} and k_{CO2}; grey scale: used for estimation of α and j_0); The following products are considered: CO(○), H2(▲), C2H4(∗), P (■). (P represents the error to 100% Faradaic efficiency in experimental data on Ag-electrode and the additional products on the Cu-electrode.)

The simulation results at low current densities are the same as in Section 3.3.1 supporting the assumption that no transport limitations occur at low current densities. Note that the experimental data for the current efficiencies does not reach 100% Faradaic efficiency for all data sets (indicated via squares in the

figures). This discrepancy is not taken into account for the Ag-electrode, which may lead to the mismatch in current efficiencies at low current densities. For GAPe with an Ag-electrode, the experimental data of higher current densities shows higher cathode potentials than predicted by the simulation results. This implies that further overpotentials occur in the experimental setup, such as an additional ohmic loss or electrode coverage due to bubble formation. This potentially leads to the discrepancy in the current efficiencies between simulated and experimental data for high current efficiencies.

The course of the simulated current efficiency towards H_2- and towards C_2H_4-production in GAPe, shown in Figure 4, are opposite to the experimental course where hydrogen production remains low and instead C_2H_4-production increases towards higher current densities. This discrepancy may have different reasons: (i) the estimated parameters partly have large confidence intervals and therefore could not be identified. Therefore, the true electrochemical reaction parameter values may differ from the values that were determined in this study and may predict the current efficiency towards higher current densities better. To overcome the issue of non-identifiability, more experimental data would be needed. (ii) A second potential reason for not finding the real parameters is that parameter estimation in gPROMS is based on a local optimization. Depending on the problem, the solution then depends on the initial values. Therefore, a better set of parameter values may be found when better initial values are given to the problem formulation, or a global optimization is conducted. (iii) A further reason may be on the modeling level, as phenomena may occur in the real reactor that are not taken into account in the model such as side reactions having an influence on the electrode potential. (iv) A further reason may be the weighting of the data in the parameter estimation via the definition of variance models in gPROMS. If all parameters are determined all at once solely for one setup and one cathode, the trend can be better represented with the herein chosen settings as shown in the Appendix. However, the confidence intervals are high and the parameter values for one system should be true in general. E.g.

the reaction parameters for the same reactive system (e.g. for one electrode and specific reactive species) should be applicable in general.

The parameter D_{Ref} is a lumped mass transport parameter assumed to be the same for all species. The parameter k_{CO2} only has an influence on the concentration of CO_2. Considering CO_2 Reduction on an Ag-electrode, Figure 4 reveals a lower total production of H_2 in a GAPe-halfcell than in a GAPc-halfcell. As the reaction parameters are the same in both setups, the lower H_2 production has to be due to a worse mass transport through the bulk and thus a lower value of D_{ref}. These results therefore suggest that the additional liquid stream trough the bulk phase of the GAPe-halfcell leads to reduced mass transport of the hydrogen ions through the electrolyte from the membrane to the cathode. Considering k_{CO2} it has to be pointed out that these values have different units for the different reactor setups as in GAPc it describes the gassing in of CO_2 from the bottom of the electrolyte and in GAPe through the GDE. A direct comparison of the values is therefore not possible. It also has to be noted, that due to the deviation of the simulated current efficiencies towards H_2-, C_2H_4-production in GAPe and its experimental courses, the highest contribution towards the objective function came from the evaluation of the corresponding current densities. In order to achieve good simulation results for the remaining variables under examination, the influence of these two electrochemical reactions in the objective function for the Cu-electrode were reduced in the combined parameter estimation of the transport parameters in the GAPe-halfcell for both electrodes.

The high values of the mass transport parameters in GAPc lead to a rather small change in concentration of the most important species H_2 and CO_2 so that also the pH in the simulation only changes from $pH_0 = 6.7$ at the beginning to pH= 7.1. The simulated and experimentally predicted pH change from pH= 5.5 to pH$\sim$ 7 indicates the worse mass transport in GAPe. Although the CO_2 dissolution parameter k_{CO2} is much lower in GAPe, the CO_2-concentration in GAPe remains higher than in GAPc throughout the whole experiment. Also

it has to be noted that both parameters represent a combination of different transport phenomena. Further analyses need to be carried out to reveal the underlying crucial phenomena that are the most influencing.

This strategy of combining experimental data of different reactors allows for parameter estimation with smaller confidence intervals. Nevertheless, the confidence values are still high so it must be said that the parameters could not be identified even with this two-stage approach and further work is needed.

3.4 Complete Reactor Comparison

The above described halfcells can be assembled to represent a complete electrochemical reactor. This allows for analysis of the overpotential distribution of one complete electrolyzer uncovering improvement approaches.

3.4.1 CO2 Reduction with GAPb-GAPe Reactor

At first we analyze the assembly of GAPe at the cathode with GAPb at the anode. All parameters are taken from the previous parameter estimations. For the anodic halfcell, it is assumed that the transport parameters of the cathodic GAPc-halfcell are the same as in all halfcells with the same design and size, so also for GAPb whose only difference to GAPc is the usage of a solid electrode. The geometric parameters are taken from the SI (Table 1).

Figure 5 (left) presents the total cell potential over the current density. Figure 5 (right) presents the Current Efficiencies (as the cathodic halfcell was already studied before, this plot is the same as in Figure 4 for halfcell GAPc with an Ag-electrode.

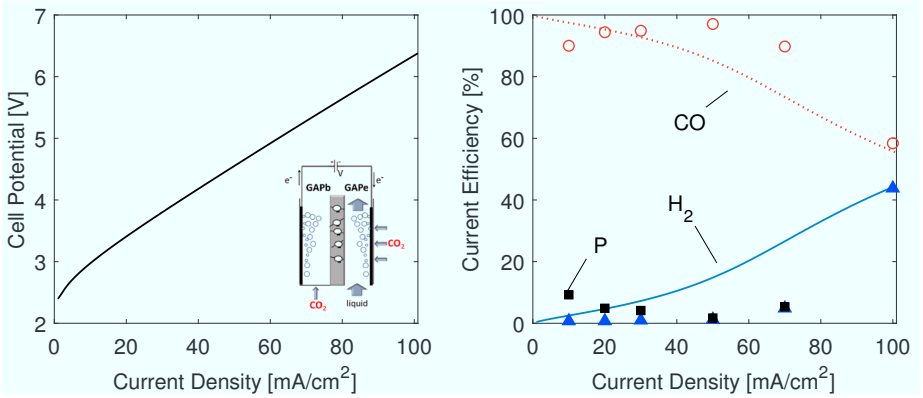

Fig. 5: Polarisation curve and Current Efficiencies for completely assembled reactor with GAPb-halfcell at anodic side and GAPe-halfcell at cathodic side with Ag-electrode of experiment[39] and simulation. The following products were taken into account: CO(○), H2(▲), P (■). (P is the error to 100% Faradaic efficiency in experimental data.)

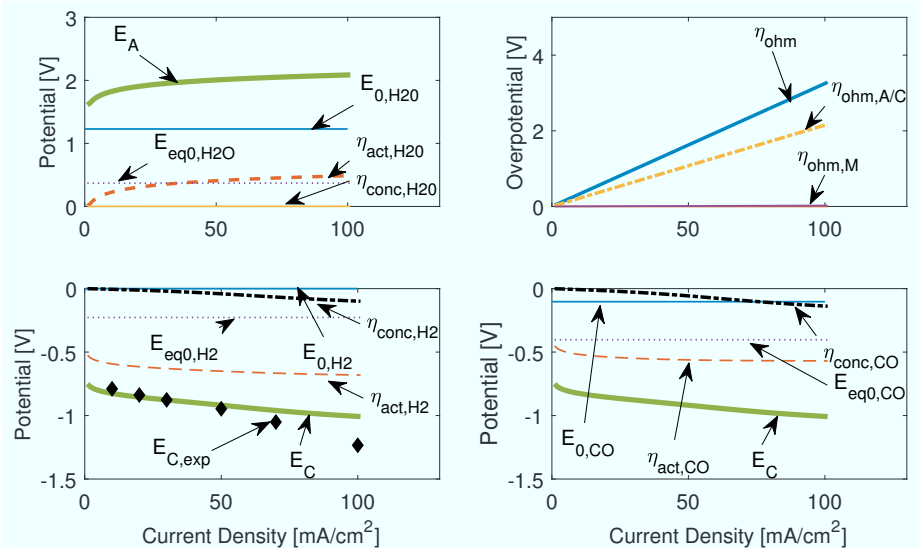

Fig. 6: Potential distribution of completely assembled cell of GAPb at anodic side and GAPe at cathodic side with Ag-electrode. Top left: potentials at anodic side; top right: ohmic potentials; bottom left: potentials at cathodic side related to H_2-production; bottom right: potentials at cathodic side related to CO-production.

The potential distribution of the completely assembled cell, as presented in Figure 6, shows that at low current densities, the standard reduction potential dominates at the anode. At the cathode, the activation overpotentials dominate with similar values for H_2- and CO-production. In the model, the course of the activation overpotential η_{act} over the current density is influenced by the Butler Volmer parameters α and j_0, but not affected by mass transport or other effects occurring in the reactor. The similar rise in concentration overpotential for H_2- and CO-production is due to the strong change in H^+-concentration, although CO_2-concentration also decreases significantly. Towards higher current densities, the influence of the ohmic resistance increases significantly which is mainly due to the ohmic resistance of the electrolytes in both halfcells $\eta_{ohm,A}$ and $\eta_{ohm,C}$.

3.4.2 CO2 Reduction with PEM-GAPe Reactor

A major goal of cell designs is to minimize ohmic overpotential. Utilization of a PEM-design or so called zero gap designs minimize the ohmic overpotential by minimizing the distance between the electrodes[30]. To reduce the overall cell potential seen in the previously shown assembly, therefore, Vennekoetter et al.[39] replace the anodic GAP-halfcell by a PEM-halfcell and reduce the GAP-width of the cathodic halfcell from 20mm to 0.5mm (which in Vennekoetter et al.[39] is called GAPf). The significantly reduced total cell potential can be seen in the experimental and simulative results presented in Figure 7. Note that the experiments were conducted with a PTFE-bonded GDE at the cathode, whereas the simulative predictions rely on electrochemical reaction parameters determined for a Nafion-bonded cathode in Section 3.3.1. This may be the reason for a slight discrepancy in the current efficiencies and the underestimation of the predicted total cell potential. Note again that the experimental data for the current efficiencies does not reach 100% Faradaic efficiency for all data sets, especially for low current densities. Furthermore, the experimental data for the current efficiency of CO indicates a maximum at ca. 30 mA/cm^2. From our understanding, current efficiencies of CO should start at a high constant level at low potentials and then decrease at high potentials like we see in the simulation. The mismatch might be due to measurement inaccuracies at low current densities where measuring the small gas flows is especially difficult.

As already mentioned above, additional ohmic overpotentials may also occur due to a change in ohmic resistivity of the electrolyte at different cell potentials or due to bubble formation. Figure 8 shows that an additional ohmic resistance with a resistivity of 0.7Ω would lead to an additional ohmic overpotential $\eta_{ohm,add}$. This would result in a good agreement of the predicted and experimental total cell potential as shown in Figure 7. The technical datasheet of the employed GDL Freudenberg H2315 I2 C6[11] states an in-plane electrical resistance of 0.7Ω. This may be the justification of the additional resistance.

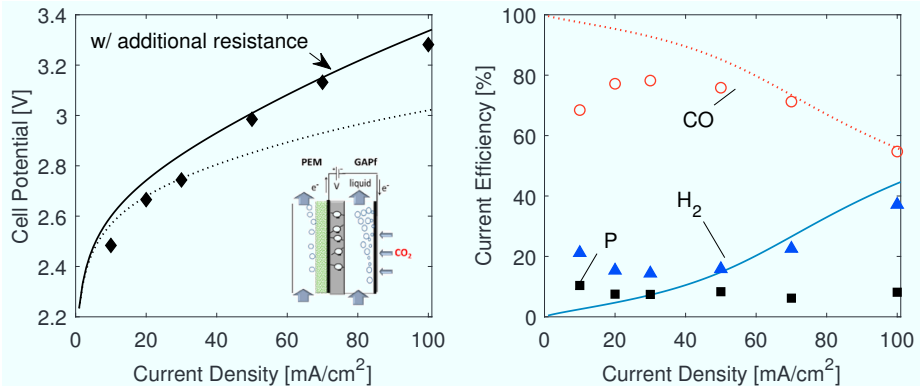

Fig. 7: Polarisation curve and Current Efficiencies for completely assembled reactor with PEM at anodic side and GAPe at cathodic side with Ag-electrode and reduced gap-width of experiment[39] and simulation. The following products were taken into account: CO(○), H2(▲), P (■). (P is the error to 100% Faradaic efficiency in experimental data.) Dashed line represents total cell potential when additional resistance is included.

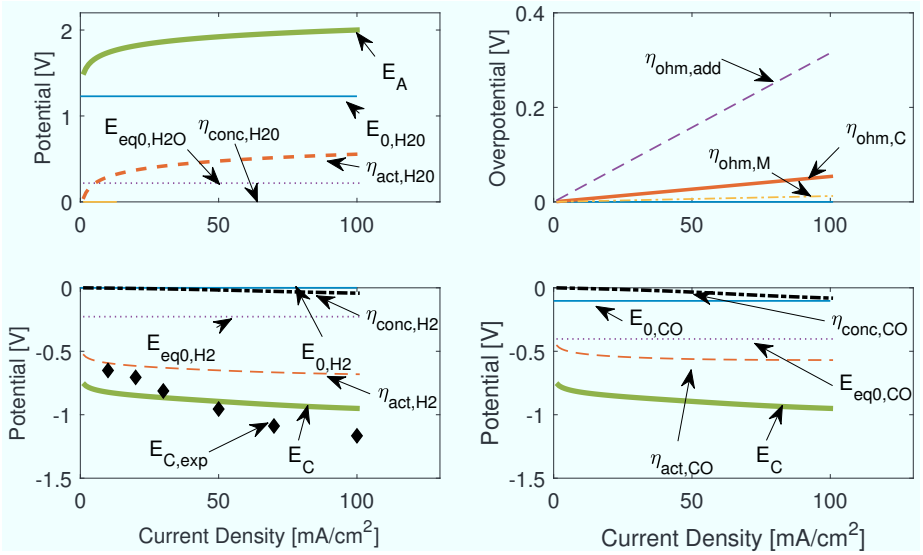

Fig. 8: Potential distribution of completely assembled cell of PEM at anodic side and GAPf at cathodic side with Ag-electrode. Top left: potentials at anodic side; top right: ohmic potentials (Dashed line represents additional resistance that may be considered for matching the total cell potential.); bottom left: potentials at cathodic side related to H_2-production; bottom right: potentials at cathodic side related to CO-production.

4 Conclusion

We developed modular mechanistic dynamic models that can be assembled to represent widely used as well as advanced cell setups in order to assess the performance and optimization potentials of these processes. The models include relevant overpotentials such as ohmic overpotentials and mass transport limitations in order to show their impact on energy losses, especially towards higher cell potentials. The models are applied to CO_2 reduction in different cell setups. We estimate electrochemical reaction parameters for CO_2 reduction on Ag- and Cu-electrodes in different halfcell setups, as well as lumped mass transport parameters. The experimental data is in most cases (but not all) well predicted. However, we show that the typically gathered experimental data - polarization plots without asymptotic part of transport limitation - is not sufficient in order to identify the parameters. The combination of experimental data for different setups and electrodes for parameter estimation decreases the confidence intervals. In future work, an identifiability analysis needs to be conducted. Moreover, optimal experimental design may help in designing the most promising future experiments leading to identification of the unknown parameters. More data is also needed in order to include and correctly parameterize the electrode coverage by bubble formation.

The assembly of the modular models to complete ecMR's results in matching simulated and experimental data. The assembled models allow analysis and detailed comparison of overpotential distribution identifying dominant loss terms of the reactor setups and indicating reactor improvements.

5 Acknowledgement

The study was conducted under the project Sustainable Chemical Synthesis (SusChemSys), which is co-financed by the European Regional Development Fund (ERDF) and the state of North Rhine-Westphalia, Germany. The authors gratefully acknowledge the financial support of the Kopernikus-project

„SynErgie“ by the Federal Ministry of Education and Research (BMBF) and the project supervision by the project management organization Projektträger Jülich (PtJ). We are also grateful to Jan-Bernd Vennekoetter, Kristina Baitalow and Matthias Hesselmann for valuable discussions. We would also like to thank the students Tony Rosemann, Alexandra Weber, Lukas Schoell, Tim Varelmann, Philipp Droste and Tobias Schiekel, who have worked on preliminary studies that helped leading to this manuscript or that used or worked on parts of the model in their student thesis and thus helped establishing the model.

References

[1] Database llnl taken from: ‘thermo.com.V8.R6.230’ prepared by Jim Johnson at Lawrence Livermore National Laboratory, in Geochemist’s Workbench format. Converted to PhreeqC format by Greg Anderson with help from David Parkhurst (llnl.dat 4023 2010-02-09 21:02:42Z dlpark).

[2] A.Bardow and M. Wessling. Converting two wastes to value. *Nature Energy*, 4(6):440–441, 2019.

[3] Aqion. www.aqion.de; last accessed: 13th June 2019.

[4] E. Bertheussen, A. Verdaguer-Casadevall, D. Ravasio, J. H. Montoya, D. B. Trimarco, C. Roy, S. Meier, J. Wendland, J. K. Nørskov, I. E. L. Stephens, and I. Chorkendorff. Acetaldehyde as an Intermediate in the Electroreduction of Carbon Monoxide to Ethanol on Oxide-Derived Copper. *Angewandte Chemie*, 128(4):1472–1476, 2016.

[5] R. Bhandari, C. A. Trudewind, and Z. Petra. Life Cycle Assessment of Hydrogen Production Methods - A Review. *STE Research Report*, 2012.

[6] A. Botz, J. Clausmeyer, D. Öhl, T. Tarnev, D. Franzen, T. Turek, and W. Schuhmann. Die lokalen Aktivitäten von Hydroxidionen und Wasser bestimmen die Funktionsweise von auf Silber basierenden Sauerstoffverzehrkathoden. *Angewandte Chemie*, 130(38):12465–12469, 2018.

[7] L. C. Brée, T. Schiekel, and A. Mitsos. Overpotentials in Water Electrolysis: In-Silico Comparison of PEM-cell and GAP-cell performance. *Proceedings of the 29th European Symposium on Computer Aided Process Engineering*.

[8] K. E. Brenan, S. L. Campbell, and L. R. Petzold. *Numerical Solution of Initial-Value Problems in Differential-Algebraic Equations*. Society for Industrial and Applied Mathematics, 1995.

[9] M. Carmo, D. L. Fritz, J. Mergel, and D. Stolten. A comprehensive review on PEM water electrolysis. *International Journal of Hydrogen Energy*, 38(12):4901–4934, 2013.

[10] E. L. Clark, J. Resasco, A. Landers, J. Lin, L. T. Chung, A. Walton, C. Hahn, T. F. Jaramillo, and A. T. Bell. Standards and Protocols for Data Acquisition and Reporting for Studies of the Electrochemical Reduction of Carbon Dioxide. *ACS Catalysis*, 8(7):6560–6570, 2018.

[11] Freudenberg gas diffusion layers technical datasheet and last accessed: 25th Aug, 2019. https://www.fuelcellstore.com/spec-sheets/freudenberg-gdl-technical-data.pdf.

[12] FuelCellStore, Technical Data Sheet - fumapem F-14100, https://fuelcellstore.com/spec-sheets/fumapem-f-14100-technical-specifications.pdf, last accessed: 30th Aug, 2019.

[13] G. Gahleitner. Hydrogen from renewable electricity: An international review of power-to-gas pilot plants for stationary applications. *International Journal of Hydrogen Energy*, 38(5):2039–2061, 2013.

[14] M. Gattrell, N. Gupta, and A. Co. A review of the aqueous electrochemical reduction of CO2 to hydrocarbons at copper. *Journal of Electroanalytical Chemistry*, 594(1):1–19, 2006.

[15] S. Ge, X. Li, B. Yi, and I.-M. Hsing. Absorption, Desorption, and Transport

of Water in Polymer Electrolyte Membranes for Fuel Cells. *Journal of The Electrochemical Society*, 152(6):A1149, 2005.

[16] GESTIS-Stoffdatenbank, 2019.

[17] M. Götz, J. Lefebvre, F. Mörs, A. McDaniel Koch, F. Graf, S. Bajohr, R. Reimert, and T. Kolb. Renewable Power-to-Gas: A technological and economic review. *Renewable Energy*, 85:1371–1390, 2016.

[18] C. H. Hamann and W. Vielstich. *Elektrochemie*. Wiley-VCH, Weinheim, 4 edition, 2005.

[19] H. Hashiba, S. Yotsuhashi, M. Deguchi, and Y. Yamada. Systematic Analysis of Electrochemical CO_2 Reduction with Various Reaction Parameters using Combinatorial Reactors. *ACS combinatorial science*, 18(4):203–208, 2016.

[20] Y. Hori. Electrochemical CO2 Reduction on Metal Electrodes. In C. G. Vayenas, R. E. White, and M. E. Gamboa-Aldeco, editors, *Modern Aspects of Electrochemistry*, pages 89–189. Springer New York, New York, NY, 2008.

[21] S. K. Kim, Y.-J. Zhang, H. Bergstrom, R. Michalsky, and A. Peterson. Understanding the Low-Overpotential Production of CH 4 from CO 2 on Mo 2 C Catalysts. *ACS Catalysis*, 6(3):2003–2013, 2016.

[22] R. Kortlever, J. Shen, K. J. P. Schouten, F. Calle-Vallejo, and M. T. M. Koper. Catalysts and Reaction Pathways for the Electrochemical Reduction of Carbon Dioxide. *The Journal of Physical Chemistry Letters*, 6(20):4073–4082, 2015.

[23] K. P. Kuhl, E. R. Cave, D. N. Abram, and T. F. Jaramillo. New insights into the electrochemical reduction of carbon dioxide on metallic copper surfaces. *Energy & Environmental Science*, 5(5):7050, 2012.

[24] W. Li, M. Seredych, E. Rodríguez-Castellón, and T. J. Bandosz. Metal-free Nanoporous Carbon as a Catalyst for Electrochemical Reduction of CO2 to CO and CH4. *ChemSusChem*, 9(6):606–616, 2016.

[25] M. Ma, K. Djanashvili, and W. A. Smith. Controllable Hydrocarbon Formation from the Electrochemical Reduction of CO2 over Cu Nanowire Arrays. *Angewandte Chemie (International ed. in English)*, 55(23):6680–6684, 2016.

[26] H. Miao, X. Xia, A. S. Perelson, and H. Wu. On Identifiability of Nonlinear ODE Models and Applications in Viral Dynamics. *SIAM review. Society for Industrial and Applied Mathematics*, 53(1):3–39, 2011.

[27] S. Motupally, A. Becker, and J. Weidner. Diffusion of Water in Nafion 115 Membranes. *Journal of The Electrochemical Society - J ELECTROCHEM SOC*, 147, 2000.

[28] J. S. Newman and K. E. Thomas-Alyea. *Electrochemical systems: Third Edition*. J. Wiley, Hoboken and N.J, 3 edition, 2004.

[29] T. V. Nguyen. A Water and Heat Management Model for Proton-Exchange-Membrane Fuel Cells. *Journal of The Electrochemical Society*, 140(8):2178, 1993.

[30] R. Phillips, A. Edwards, B. Rome, D. R. Jones, and C. W. Dunnill. Minimising the ohmic resistance of an alkaline electrolysis cell through effective cell design. *International Journal of Hydrogen Energy*, 42(38):23986–23994, 2017.

[31] L. Plummer and E. Busenberg. The solubilities of calcite, aragonite and vaterite in CO2-H2O solutions between 0 and 90°C, and an evaluation of the aqueous model for the system CaCO3-CO2-H2O. *Geochimica et Cosmochimica Acta*, 46(6):1011–1040, 1982.

[32] Process Systems Enterprise, gPROMS, www.psenterprise.com/gproms, 1997-2018.

[33] D. Raciti, K. J. Livi, and C. Wang. Highly Dense Cu Nanowires for Low-Overpotential CO 2 Reduction. *Nano Letters*, 15(10):6829–6835, 2015.

[34] F. Roghmans, M. C. Martí-Calatayud, S. Abdu, R. Femmer, R. Tiwari, A. Walther, and M. Wessling. Electrochemical impedance spectroscopy fingerprints the ion selectivity of microgel functionalized ion-exchange membranes. *Electrochemistry Communications*, 72:113–117, 2016.

[35] A. Rommerskirchen, A. Kalde, C. J. Linnartz, L. Bongers, G. Linz, and M. Wessling. Unraveling charge transport in carbon flow-electrodes: Performance prediction for desalination applications. *Carbon*, 145:507–520, 2019.

[36] F. J. W. Roughton and V. H. Booth. The catalytic effect of buffers on the reaction CO_2+H(2)O⇌H(2)CO(3). *Biochemical Journal*, 32(11):2049–2069, 1938.

[37] B. Schmid, C. Reller, S. Neubauer, M. Fleischer, R. Dorta, and G. Schmid. Reactivity of Copper Electrodes towards Functional Groups and Small Molecules in the Context of CO2 Electro-Reductions. *Catalysts*, 7(5):161, 2017.

[38] C. W. Tobias, M. Eisenberg, and C. R. Wilke. Fiftieth Anniversary: Diffusion and Convection in Electrolysis—A Theoretical Review. *Journal of The Electrochemical Society*, 99(12):359C, 1952.

[39] J.-B. Vennekoetter, R. Sengpiel, and M. Wessling. Beyond the catalyst: How electrode and reactor design determine the product spectrum during electrochemical CO2 reduction. *Chemical Engineering Journal*, 364:89–101, 2019.

[40] S. Verma, S. Lu, and P. J. Kenis. Co-electrolysis of co 2 and glycerol as a pathway to carbon chemicals with improved technoeconomics due to low electricity consumption. *Nature Energy*, page 1, 2019.

[41] É. Walter and L. Pronzato. *Identification of parametric models from experimental data*. Communications and control engineering series. Springer, London, 1997.

[42] O. Walz, C. Marks, J. Viell, and A. Mitsos. Systematic approach for modeling reaction networks involving equilibrium and kinetically-limited reaction steps. *Computers & Chemical Engineering*, 98:143–153, 2017.

[43] W. Wang, X. Wei, D. Choi, X. Lu, G. Yang, and C. Sun. Chapter 1 - Electrochemical cells for medium- and large-scale energy storage: fundamentals. In C. Menictas, M. Skyllas-Kazacos, and T. M. Lim, editors, *Advances in Batteries for Medium and Large-Scale Energy Storage*, Woodhead Publishing Series in Energy, pages 3–28. Woodhead Publishing, 2015.

[44] L. C. Weng, A. T. Bell, and A. Z. Weber. Towards membrane-electrode assembly systems for CO2 reduction: A modeling study. *Energy and Environmental Science*, 12(6):1950–1968, 2019.

[45] D. Wiley and G. Fimbres Weihs. Electroosmotic Drag in Membranes. In E. Drioli and L. Giorno, editors, *Encyclopedia of Membranes*, pages 653–654. Springer Berlin Heidelberg, Berlin, Heidelberg, 2016.

[46] J. Wu and X.-D. Zhou. Catalytic conversion of CO2 to value added fuels: Current status, challenges, and future directions. *Chinese Journal of Catalysis*, 37(7):999–1015, 2016.

[47] X. Yang, F. Karnbach, M. Uhlemann, S. Odenbach, and K. Eckert. Dynamics of Single Hydrogen Bubbles at a Platinum Microelectrode. *Langmuir*, 31(29):8184–8193, 2015.

[48] F. Zhou, S. Al Shakhshir, and S. K. Kær. Current and Temperature Distribution Measurement in a Polymer Electrolyte Membrane Water Electrolyzer Cell. *ECS Transactions*, 85(13):1005–1012, 2018.

Appendix

Dissociation constants for pH-calculation

$$K_{pH}(\text{eq.15}) = 10^{-14} \tag{23}$$

$$K_{pH}(\text{eq.16}) = 10^{6.05} \tag{24}$$

$$K_{pH}(\text{eq.17}) = 10^{6.35}\,[31] \tag{25}$$

$$K_{pH}(\text{eq.18}) = 10^{10.33}\,[31] \tag{26}$$

$$K_{pH}(\text{eq.19}) = 10^{6.3}\,[3] \tag{27}$$

$$K_{pH}(\text{eq.20}) = 10^{1.9791}\,[1] \tag{28}$$

Potassium belongs to the group of alkali metals and sulfuric acid is a very strong acid. Therefore, potassium and sulfuric acid dissociate completely according to Eq.21.

Parameters for each Halfcell

Table 1: Parameters used in the simulations.

Parameter	Description	Value		Unit	Reference
general values					
p	pressure of system	10^5		[Pa]	
T	temperature of system	293.15		[K]	
Butler-Volmer parameters for water splitting at anode:					
α_{an}	transfer cofficient at anode	0.89		[-]	[7]
$j_{0,an}$	exch. current density anode	7.16		[A.m^{-2}]	[7]
solubility in water					
$c_{0,CO}$	solubility at 20°C	30		[mg.l^{-1}]	[16]
$c_{0,CH4}$	solubility at 25°C	22.5		[mg.l^{-1}]	[21]
$c_{0,H2}$	solubility at 20°C	30		[mg.l^{-1}]	[16]
$c_{0,C2H4}$	solubility at 20°C	130		[mg.l^{-1}]	[16]
$c_{0,P}$	solubility at 20°C	$1{\cdot}10^{-4}$		[mol.m^{-3}]	assumption
PEM					
x_{GDL}	thickness of GDL	$250{\cdot}10^{-6}$		[m]	
y_{GDL}	hight of GDL	0.04		[m]	A_{active} = 20cm^2 [39]
z_{GDL}	depth of GDL	0.05		[m]	A_{active} = 20cm^2 [39]
ϵ_{GDL}	porosity of GDL	0.46		[-]	
τ_{GDL}	tortuosity of GDL	5		[-]	
D_{ref}	mass transport coeff.	$1{\cdot}10^{-9}$		[m^2.s^{-1}]	
a_i	activity of the species	1		[]	
GAP		GAPb/c	GAPe		
ss_{CO2}	side stream of CO_2	0	1	[-]	
bs_{CO2}	bottom stream of CO_2	1	0	[-]	
x_{GAP}	thickness of GAP	0.02	0.02	[m]	[39]
(x_{GAP})	(thickness of GAP in Sec. 3.4.2)	–	0.0005	[m]	[39]
y_{GAP}	height of GAP at Cathode	0.03[b]	0.03	[m]	A_{active} = 4.5cm^2 [39]
z_{GAP}	depth of GAP at Cathode	0.015[b]	0.015	[m]	A_{active} = 4.5cm^2 [39]
κ_{GAP}	conductivity of electrolyte	9.3	9.3	[S.m^{-1}]	[39]
D_{ref}	mass transport coeff.	0.035	0.0025	[m^2.s^{-1}]	Table 4
k_{CO2}	mass transport coeff.	37,500	–	[s^{-1}]	Table 4
k_{CO2}	mass transport coeff.	–	$1.1{\cdot}10^{-3}$	[m^3.s^{-1}]	Table 4
Membrane					
x_M	thickness of Membrane	$115{\cdot}10^{-6}$		[m]	[12] (swelling consid.)
y_M	hight of Membrane	0.03		[m]	
z_M	depth of Membrane	0.03		[m]	
κ_M	conductivity	9.3		[S.m^{-1}]	[39]
ξ_M	electro-osmotic-drag	2.5		[m]	
$D_{bd,M}$	diffusion coeff. of H_2O	$1.05{\cdot}10^{-10}$,[a]		[m^2.s^{-1}]	[27, 29]

[a]: $D_{bd,M}$ is calculated for the given temperature and a water content of the membrane $\lambda = 22$.
[b]:When used as the anode, the values for height and depth were y_{GAP}=0.03 z_{GAP}=0.03, respectively, for A_{active} = 9cm^2 [39].

Extrapolation of the experimental pH-values to determine the value at zero current

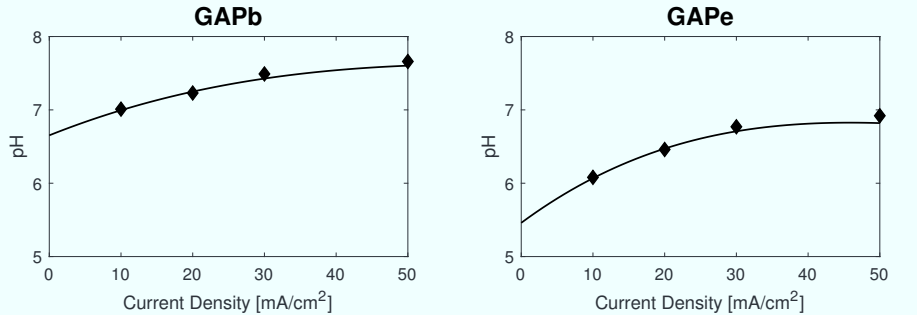

Fig. 9: Experimentally determined pH-values[39] in the bulk phase of setups GAPb and GAPe

plotted with their approximated course over current density. At j=0mA/cm^2 pH_0 is taken.

Parameters Determined for CO_2 Reduction in GAPc-Halfcell with Cu-Electrode

Table 2: Estimated model parameters for CO_2 reduction in GAPc with a Cu-electrode

Parameter	Unit	Final Value	95% confidence interval
Cu GAPc			
$\alpha_{H2,Cu}$	[-]	0.69	0.015
$\alpha_{CO,Cu}$	[-]	0.06	0.04*
$\alpha_{C2H4,Cu}$	[-]	0.33	0.008
$\alpha_{extra,Cu}$	[-]	0.24	0.008
$j_{0,H2,Cu}$	[Am^{-2}]	$5.83{\cdot}10^{-10}$	0.006*
$j_{0,CO,Cu}$	[Am^{-2}]	16.64	$1.4{\cdot}10^{-8}$*
$j_{0,C2H4,Cu}$	[Am^{-2}]	$2.31{\cdot}10^{-8}$	0.026*
$j_{0,extra,Cu}$	[Am^{-2}]	0.113	0.026*
D_{ref}	[m^2s^{-1}]	0.047	0.0001
k_{CO2}	[s^{-1}]	48952	23990*

*large confidence interval

Parameters Determined in the 2-Stage Parameter Estimation

Table 3: Electrochemical reaction parameters estimated for each electrode (Cu and Ag)

Parameter	Unit	Final Value	95% confidence interval
Ag Nafion-bonded electrode			
$\alpha_{H2,Ag}$	[-]	0.74	0.05
$\alpha_{CO,Ag}$	[-]	0.43	0.033
$j_{0,H2,Ag}$	[Am^{-2}]	$1.71{\cdot}10^{-15}$	$4.74{\cdot}10^{-15}$*
$j_{0,CO,Ag}$	[Am^{-2}]	$2.12{\cdot}10^{-6}$	$2.95{\cdot}10^{-6}$*
Cu Nafion-bonded electrode			
$\alpha_{H2,Cu}$	[-]	0.83	0.08
$\alpha_{CO,Cu}$	[-]	0.18	0.009
$\alpha_{C2H4,Cu}$	[-]	0.36	0.12
$\alpha_{P,Cu}$	[-]	0.08	0.01
$j_{0,H2,Cu}$	[Am^{-2}]	$8.9{\cdot}10^{-14}$	$3.3{\cdot}10^{-13}$*
$j_{0,CO,Cu}$	[Am^{-2}]	0.31	0.09
$j_{0,C2H4,Cu}$	[Am^{-2}]	$1.23{\cdot}10^{-10}$	$1.01{\cdot}10^{-9}$*
$j_{0,P,Cu}$	[Am^{-2}]	2.93	1.3

*large confidence interval

Table 4: Mass transport kinetic parameters estimated for GAPc and GAPe.

Parameter	Unit	Final Value	95% confidence interval
GAPc			
D_{ref}	[m^2s^{-1}]	0.043	0.006
k_{CO2}	[s^{-1}]	85,204	41,660*
GAPe			
D_{ref}	[m^2s^{-1}]	0.0025	0.0005
k_{CO2}	[$m^3.s^{-1}$]	$1.1{\cdot}10^{-3}$	0.01*

*large confidence interval

Parameters Determined individually for CO_2 Reduction in each Halfcell

According to the procedure in Section 3.2., parameter estimations are carried out for each reactor individually with determination of all unknown parameters at once.

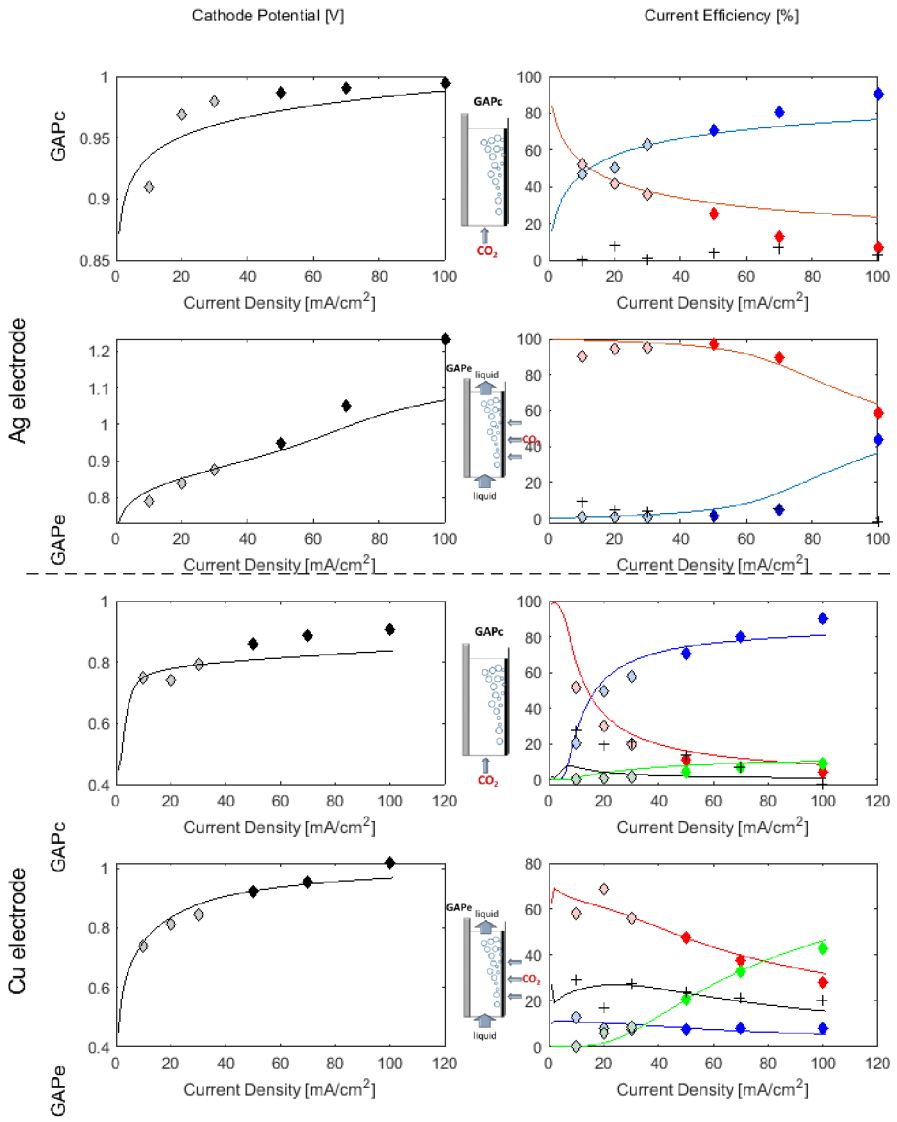

Fig. 10: Results GAPc-halfcell and GAPe-halfcell with Ag-electrode. colored ◇ is experimental data (grey scale: used for estimation of initial values for α and j_0 that are used in the parameter estiamtion); "–" CO; "–" H2; "–" C2H4; "–" HCOOH; "+" error to 100% Faradaic efficiency

Table 5: Electrochemical reaction parameters and mass tranpsort parameters estimated all at once for each reactor setup individually.

Parameter	Unit	Final Value
GAPc Ag Nafion-bonded electrode		
$\alpha_{H2,Ag}$	[-]	0.75
$\alpha_{CO,Ag}$	[-]	0.35
$j_{0,H2,Ag}$	[Am^{-2}]	19.63
$j_{0,CO,Ag}$	[Am^{-2}]	1.65
D_{ref}	[m^2s^{-1}]	0.039
k_{CO2}	[s^{-1}]	45967 *
GAPe Ag Nafion-bonded electrode		
$\alpha_{H2,Ag}$	[-]	0.70
$\alpha_{CO,Ag}$	[-]	0.05
$j_{0,H2,Ag}$	[Am^{-2}]	$5{\cdot}10^{-15}$
$j_{0,CO,Ag}$	[Am^{-2}]	$2.65{\cdot}10^{-5}$
D_{ref}	[m^2s^{-1}]	0.0008
k_{CO2}	[s^{-1}]	0.001 *
GAPc Cu Nafion-bonded electrode		
$\alpha_{H2,Cu}$	[-]	0.69
$\alpha_{CO,Cu}$	[-]	0.06
$\alpha_{C2H4,Cu}$	[-]	0.33
$\alpha_{extra,Cu}$	[-]	0.24
$j_{0,H2,Cu}$	[Am^{-2}]	$5.83{\cdot}10^{-10}$
$j_{0,CO,Cu}$	[Am^{-2}]	16.64
$j_{0,C2H4,Cu}$	[Am^{-2}]	$2.31{\cdot}10^{-8}$
$j_{0,extra,Cu}$	[Am^{-2}]	0.113
D_{ref}	[m^2s^{-1}]	0.047
k_{CO2}	[s^{-1}]	48952
GAPe Cu Nafion-bonded electrode		
$\alpha_{H2,Cu}$	[-]	0.1
$\alpha_{CO,Cu}$	[-]	0.09
$\alpha_{C2H4,Cu}$	[-]	0.16
$\alpha_{extra,Cu}$	[-]	0.16
$j_{0,H2,Cu}$	[Am^{-2}]	0.18
$j_{0,CO,Cu}$	[Am^{-2}]	1.93
$j_{0,C2H4,Cu}$	[Am^{-2}]	$5.8{\cdot}10^{-7}$
$j_{0,extra,Cu}$	[Am^{-2}]	0.35
D_{ref}	[m^2s^{-1}]	0.003
k_{CO2}	[s^{-1}]	10,000